CrystEngComm

Self-Assembly of Sodium 4-(4,5-Diphenyl-1H-imidazol-2-yl)benzoate into Ultralong Microbelts

Journal:	*CrystEngComm*
Manuscript ID:	CE-ART-03-2014-000457.R1
Article Type:	Paper
Date Submitted by the Author:	21-May-2014
Complete List of Authors:	zhao, hongyan; Xiangtan University, College of Chemistry Li, Huaming; Xiangtan University, College of Chemistry Chen, Hongbiao; Xiangtan University, College of Chemistry Gao, Yong; Xiangtan University, College of Chemistry

Self-assembly of sodium 4-(4,5-diphenyl-1H-imidazol-2-yl)benzoate into ultralong microbelts†

Hongyan Zhao[a], Hongbiao Chen[a]*, Yong Gao[a], Huaming Li[a,b]*

[a] College of Chemistry, Xiangtan University, Xiangtan 411105, Hunan Province, P. R. China

[b] Key Laboratory of Polymeric Materials & Application Technology of Hunan Province, Key Laboratory of Advanced Functional Polymeric Materials of College of Hunan Province, and Key Lab of Environment-friendly Chemistry and Application in Ministry of Education, Xiangtan University, Xiangtan 411105, Hunan Province, P. R. China

*Corresponding author. Tel.: +86 731 58298572; Fax: +86 731 58293264.

E-mail address: lihuaming@xtu.edu.cn (H. Li), chhb606@163.com (H. Chen).

Abstract

In this study, a self-assembly technique is developed to fabricate ultralong microbelts of sodium 4-(4,5-diphenyl-1H-imidazol-2-yl)benzoate (SDB). The as-prepared SDB microbelts are identified to have a belt-like structure with a rectangular cross section. All the obtained microbelts under optimal conditions have a relatively uniform size of about 5 μm in width, 2 μm in thickness, and approximately 5 mm in length. Particularly, the length of the SDB microbelts can be readily controlled by adjusting the SDB concentration as well as the aging temperature. In addition, the optical and electrical properties of the as-prepared microbelts are also investigated. These results should be significant in triarylimidazole derivatives crystallization and their potential application in optoelectronic devices.

Introduction

The self-assembly of small organic molecules into one-dimensional (1D) nano/microstructures is a powerful tool to create novel materials with peculiar properties.[1] Currently, there is a growing interest in the fabrication of organic 1D nano/micromaterials, such as wires,[1,2] belts,[3] tubes,[4-6] and rods,[6,7] in a controlled and predictable fashion. Compared with their inorganic counterparts, organic 1D nano/micromaterials have some advantages such as good processability,[8] effective doping property,[9] and high photoluminescence efficiency,[10] which make them ideal candidates for optoelectronic nanodevices. In most cases, these self-assembled 1D organic nano/microstructures in solution usually have a length that is typically in the range of nanometer-to-micrometer scale. More recently, the construction of ultralong organic 1D nano/microstructures has been reported, in which the average length ranges from several micrometers up to millimeter scale.[11,12] Such a pronounced enhancement in aspect ratio has obvious advantages in single device fabrication and measurement, which is crucial for the realization of the practical applications of these materials. As a consequence, ultralong organic 1D nano/microstructures have found potential application in areas such as optical waveguides,[13] field-effect transistors,[14] organic light emitting diodes,[15] solar cells,[16] sensors,[17] and photoswitching devices.[18]

Besides the above mentioned self-assembly approach,[19,20,21] template-based method,[22,23] and vapor deposition[24,25] have also been used to construct ultralong 1D nano/microstructures. Although the hard-template synthesis is a popular, reliable, and convenient approach for preparing ultralong 1D nano/microstructures, it is difficulty to prepare 1D structure from a small organic compound that has the same solubility properties as the used template. In addition, the inorganic template

removal process is usually energy-consuming. On the other hand, vapor deposition technique relies heavily on sophisticated instruments. In this regard, the self-assembly of small organic molecules through the use of soft template,[26] poor solvent,[27] or solvent evaporation[28] is a facile and reliable method to prepare ultralong organic 1D nano/microstructures. For example, several small organic molecules, such as 2-anthracen-9-ylmethylene malononitrile,[29] 3,4,9,10-perylenetetracarboxylic acid potassium salt (PTCAPS),[30] spiro-substituted perylenetetracarboxylic diimide (spiro-PDI),[31] 2-(3′,5′-bis(trifluoromethyl)biphenyl-4-yl)-3-(6-3,5-bis(trifluoromethyl)phenyl)pyridine-3-yl)acrylonitrile (Py-CN-TBE),[32] 2,4,6-tris(4-cyano-1,2,5-thiadiazol-3-yl)-1,3,5-triazine (TCTDT), and 2,4,6-tris(4-cyano-1,2,5-selenodiazole-3-yl)-1,3,5-triazine (TCSDT),[33] have been successfully utilized to fabricate ultralong 1D structures via solution-based self-assembly method. As can be seen, only a small percentage of known small organic compounds so far have been found to form such structures, thereby placing a restriction on the range of potential chemophysical properties.

Recently, triphenylimidazole derivatives have attracted considerable attention because of their unique photoluminescent and chemiluminescent properties[34-36] as well as their diverse biological activities.[37,38] These compounds possess a larger conjugated-system structure and can assemble into 1D structured materials through intermolecular interactions. To date, triphenylimidazole based wires,[39] rods,[40] and tubes[41] have been successfully fabricated by using various synthetic methods. These 1D nanostructures derived from triphenylimidazole derivatives have size-dependent optical properties and good stability, which allow them to find potential applications in novel optical and optoelectronic devices. Thus, acquirement of new 1D nano/microstructures, especially ultralong

belt-like structures, is desirable for the fundamental understanding of their properties as well as the realization of diverse potential applications. Herein, we describe the fabrication of the ultralong microbelts from sodium 4-(4,5-diphenyl-1H-imidazol-2-yl)benzoate (SDB) by the poor solvent mediated self-assembly method. Such method should be significant in triarylimidazole derivatives crystallization since no template or surfactant was necessary to assemble these microstructures. Moreover, the size of the as-fabricated SDB microbelts can be readily controlled by adjusting the experimental conditions. In the current study, the optical and electrical properties of the belt-like microstructures were also investigated.

Experimental section

Materials

The organic compound of SDB used in this study was synthesized in-house and was characterized by NMR and MS spectroscopy (Figs. S1-S3, see Electronic supplementary information, ESI†). Ultrapure water with a resistivity ≥ 18.2 MΩ was produced using a Milli-Q apparatus (Millipore) and was filtered using a membrane with a pore size of 200 nm (Whatman International, Ltd.) just before use. Tetrahydrofuran (THF) was obtained from Guangdong Guanghua Chemical Factory Co. Ltd., and was distilled before use.

Sample preparation method

Ultralong SDB microbelts were prepared by the simple and versatile self-assembly method. In a typical preparation, raw powder of SDB was dissolved in THF to a concentration of 3.0 mM. Then 600 μL of this solution was added dropwise into 5.0 mL ultrapure water with vigorous stirring at 50 °C. After stirring for 1 min, the suspension was left undisturbed at 30 °C to stabilize for a desired time. The micobelts were collected by filtration followed by washing several times with ultrapure water and finally dried under vacuum at 50 °C for 24 h.

Characterization

Optical microscopy measurement was performed with a Leica DM4500P microscope. Scanning electron microscope (SEM) images were recorded using a JEOL (JSM-6360LV) scanning electron microscope, and the samples were loaded on the mica surface, previously sputter-coated with a homogeneous gold layer for charge dissipation during the SEM imaging. Powder X-ray diffraction (XRD) patterns of the samples were measured on a Japan Rigaku D/max-2500 diffractometer with Cu-Kα radiation (λ = 1.5418 Å). The samples (SDB raw powder and SDB microbelts) were grinded into fine powder for XRD measurements. FTIR spectra in KBr pellets were recorded on a PE Spectrum One FTIR spectrophotometer. Fluorescence spectra were recorded on a PE LS-55 luminescence spectrometer. Fluorescence microscopic pictures were recorded using a MF30 fluorescence microscope the excitation wavelength of 330-400nm. UV-vis absorption spectra were measured using a PE Lamada 25 spectrometer (for sample preparation, see ESI†). The electrical characteristics were measured in ambient laboratory conditions by using a Keithley 4200-SCS semiconductor parameter analyzer.

Results and discussion

The self-assembly of supramolecular aggregates of SDB into ultralong belt-like structures is a poor solvent mediated process. In a typical procedure, a solution of SDB in THF (3.0 mM, 600 μL) was added dropwise into hot ultrapure water (5.0 mL, 50 °C) with vigorous stirring. After stirring for 1 min, the sample was left undisturbed at 30 °C for about 5 h to stabilize the microstructure growth. Fig. 1a and b show the digital photographs of the as-prepared microbelts. It is amazing that the belts can be seen by the naked eye (Fig. 1b) and their length reaches several millimeters (Fig. 1a). The optical micrograph of a single microbelt in Fig. 1f further demonstrates that the length reaches to about 5 mm. Fig. 1d and e show the morphology of microbelts cast on mica substrate. The SEM images clearly reveal that the product has a belt-like morphology with the thickness of about 2 ± 0.5 μm and the width of about 5 ± 0.5 μm (Fig. 1d). In addition, the rectangular shape of the cross section can also be seen from Fig. 1e inset. In order to further prove the successful fabrication of SDB ultralong microbelts, a statistical analysis is then conducted by measuring over 50 microbelts in digital photographs. The result in Fig. 1c shows that the average length of the as-synthesized SDB microbelts is around 3.5 mm. However, it should be noted that the produced microbelts are easily broken during the sample preparation process.

[Fig. 1]

The crystalline phase of the SDB microbelts was identified by powder X-ray diffraction. The XRD patterns of SDB raw powder and SDB microbelts are shown in Fig. 2. As can be seen, the sharp peaks in the XRD patterns confirm that the SDB raw powder as well as the SDB microbelts

is crystalline. Detailed analysis was performed by using the program Powder-X, and the results showed that the crystalline phases of microbelts and SDB raw powder are monoclinic. Some differences, however, are observed in their lattice parameters. The lattice parameters of the SDB microbelts are a = 17.069 Å, b = 4.349 Å, c = 14.141 Å, α = 90°, β = 112.884°, γ = 90°, and volume = 967.052 Å^3, while the cell parameters of the SDB raw powder are a = 8.617 Å, b = 12.326 Å, c = 6.402 Å, α = 90°, β = 111.348°, γ = 90°, and volume = 637.358 Å^3 (Tables S1-S2, ESI†). The differences in their cell parameters might originate from the different crystallization processes.

[Fig. 2]

Fig. 3 depicts the FITR spectrum of the as-prepared SDB microbelts, which is almost identical to that of the SDB raw powder, indicating that the SDB has not undergone other chemical reactions during the self-assembly process. This result again confirms that the microbelts consist of pure SDB materials.

[Fig. 3]

The synthesis parameters, such as the SDB concentration and aging temperature, play an important role in the microbelt length control. A series of experiments were thus performed. Firstly, the influence of SDB concentration on the produced microbelts was investigated. Fig. 4 shows the optical microscope images of the synthesized products with different SDB concentrations. In our experiments, the concentration of SDB solution in THF was varied from 2.0 mM to 4.0 mM, while the temperature and aging time were kept constant, i.e., 30 °C and 5 h, respectively. As shown in

Fig. 4, when the concentration of SDB was varied, both the length and width of the microbelts changed gradually. For example, when the concentration of SDB is 2.0 mM, the average length and width of the SDB microbelts are around 2.3 mm and 2.9 μm, respectively. As the concentration of SDB further increases, the length and width increase accordingly. At the SDB concentration of 3.0 mM, the average length and width increase to 3.5 mm and 3.9 μm, respectively, and at 4.0 mM they are 4.4 mm and 6.1 μm, respectively. It is worth noting that the microbelts still have rectangular shape feature. Since high SDB concentration will increase the supply of source molecules during seed formation and enhance the subsequent rate of crystallization and growth, which is therefore related to the microbelts length and degree of dispersion. This assembly method provides an opportunity to control the length of molecule-based materials.

[Fig. 4]

The length of the self-assembled SDB microbelts can also be tuned by changing the self-assembly temperature. In an attempt to investigate the temperature on the morphology of the SDB crystals, aging temperature was systematically varied from 30 to 0 °C while the SDB concentration (3.0 mM) and aging time (5 h) were kept constant, and their effect was evaluated by optical microscopy analysis. As shown in Fig. 5, it is possible to achieve belt-like structures (Fig. 5c-e) as the aging temperature decreases to 10 °C. However, the average length of the SDB microbelts decreases with decreasing the aging temperature. For example, the average length of the SDB microbelts is around 3.5 mm at the aging temperature of 30 °C. Conversely, the average length of the SDB microbelts decreases to 2.9 mm at the aging temperature of 20 °C, and it is 1.7

mm at the aging temperature of 10 °C. Interestingly, the belt-like structures have completely disappeared when the aging temperature decreases to 0 °C. Instead, the product exhibits a complicated shape consisting of irregular dendrite-like structures with size of several hundred micrometers (Fig. 5a-b). All these results indicate that the aging temperature plays a key role in the formation of the SDB belt-like structures.

[Fig. 5]

On the basis of the above mentioned results, the SDB should have a highly oriented nature of assembly. However, this in turn makes it difficult to obtain ideal crystal suitable for single-crystal XRD identification. By using the density functional theory (DFT), the possible packing structure of SDB molecules was proposed. The theoretical calculations were performed using the PBE functional and DND basis set implemented in DMOL3 soft package.[42,43] In Fig. S4a (see ESI†), the obtained lowest energy packing structure of SDB dimer indicates strong interactions between the NH group and $COO^{-}Na^{+}$ unit. The NH can interact with the O atom in $COO^{-}Na^{+}$ unit to form a hydrogen bond and the rest N atom in the 1,3-diazole ring interacts with the Na^{+} *via* electrostatic interactions. The calculated binding energy between two molecules is 0.56 eV. The definition of binding energy (E_b) is $E_b = [E_{dimer} - 2 \times E_{SDB}]/2$, where the E_{dimer} is the energy of molecular dimer and E_{SDB} is the energy of single SDB molecule. On basis of the packing structure of dimer aggregate, we further investigated the extended packing structure of SDB molecules. From Fig. S4b (see ESI†), the intense π-π stacking structures formed by the phenyl rings and 1,3-diazole ring are clearly found. The inter-phenyl ring distance is about 3.6 Å. The binding energy of hexamer structure is 0.72 eV per molecule, indicating the strong interactions between SDB molecules. So,

we speculate that the driving force in the self-assembled belt structure is attributed to multi factors including the hydrogen bond between NH and $COO^{-}Na^{+}$, the electrostatic interactions between N atom (in 1,3-diazole ring) and $COO^{-}Na^{+}$ group, as well as the π-π stacking effects of conjugated rings.

The optical properties of the as-prepared SDB microbelts dispersed in water were also investigated. Considering that the microbelts are easily broken, the as-prepared SDB microbelts suspended in water were directly diluted with water to obtain a suitable microbelt concentration for optical measurements. Fig. 6 displays the UV-vis absorption spectra of the SDB microbelts with different lengths dispersed in water. For comparison, the spectra of SDB raw powder dispersed in water as well as dissolved in THF are also displayed. The dilute solution of SDB in THF is colorless and shows an absorption band with a peak at 341 nm, which originates from the electronic transition from HOMO to LUMO+2.[44] However, the absorption spectrum of SDB raw powder dispersed in water shows a main characteristic band at 316 nm, giving a hypsochromic shift of 25 nm compared to that of SDB solution. This indicates that the main interaction changes from intramolecular to intermolecular electronic transition.[45] Similarly, the UV-vis spectra of SDB microbelts dispersed in water also show absorption bands with peaks at around 310 nm. Through a careful observation of Fig. 6, however, the as-fabricated SDB microbelts show interesting size dependent optical properties. When the length of the microbelts increases from 2.5 to 4.4 mm, the absorption band appears at around 307 nm and is gradually red shifted to approximately 313 nm. This is expected for an aggregate state arising from the π–π orbital overlap of closely stacked SDB molecules.[46] As the microbelts size increases, the degree of the π–π orbital overlap will be enhanced and thus will result in its absorption shifting to a lower energy. In order to eliminate the

possibility of concentration effect, concentration dependent UV-vis spectra of SDB microbelts dispersed in water as well as the solution of SDB in THF were then performed. As expected, the absorbance increases with increasing SDB or SDB microbelts concentrations. However, no change in the wavelength of maximum absorbance is observed when their concentrations increase (Fig. S5, ESI†). For the purpose of further investigating the optical properties of SDB aggregate, solid state UV-vis spectra of SDB monomer as well as SDB microbelts were thus measured. The sample was prepared by spin coating SDB solution in THF or SDB microbelts suspension in water onto clear quartz slide at 2000 rpm. Solid state UV-vis spectral study shows that SDB monomer and SDB microbelts have broader absorption bands with peaks at 330 and 345 nm, respectively (Fig. S6, ESI†).

[Fig. 6]

The fluorescence spectra of the SDB microbelts dispersed in water with different lengths are shown in Fig. 7. Similarly, the fluorescence spectra of SDB raw powder dispersed in water as well as dissolved in THF are also displayed for comparison. The fluorescence spectrum of SDB in solution shows an emission band with maximum at 420 nm. However, the fluorescence spectrum of SDB raw powder dispersed in water shows a characteristic band at 435 nm, giving a bathochromic shift of 15 nm compared to that of SDB solution. This may be attributed to the π-π interactions[47] as well as the inner filter effects[48] due to the high local concentration of SDB powder. Similarly, the fluorescence spectra of SDB microbelts dispersed in water also show emission bands with peaks at around 436 nm. Again, the size dependent properties are observed for the SDB microbelts. For example, the emission band appears at around 436 nm and is gradually redshifted

to approximately 443 nm as the length of the microbelts increases from 2.5 to 4.4 mm (Fig. 7). In addition, concentration dependent fluorescence spectra as well as fluorescence images of the SDB solution in THF were then performed (Figs. S7-S8, ESI†). As expected, the emission intensity increases with increasing SDB powder or SDB microbelts concentrations. Again, no change in the peak emission wavelength is observed when their concentrations increase (Fig. S7, ESI†). In this study, solid state fluorescence spectra of SDB monomer as well as SDB microbelts were also measured. Clearly, the sample in solid state leads to a suppression of the fluorescence intensity. The SDB monomer and SDB microbelts show emission bands with peaks at 425 and 424 nm, respectively (Fig. S9, ESI†).

[Fig. 7]

The extended π-π interactions in the SDB microbelts promoted us to investigate their electrical properties. The electrical conductivity measurements of the as-fabricated SDB microbelts were carried out using a semiconductor parameter analyzer. The devices were fabricated by pasting a pair of conductive double-sided sticky carbon tape onto Si/SiO_2 substrate with a gap ranging from 0.8 to 1.0 mm, followed by attaching the SDB microbelts to link the two tape electrodes. Typical current–voltage (*I–V*) curves of the SDB microbelts in the dark and under light illumination are shown in Fig. 8 (inset shows a schematic diagram of a top-contact device). The power of the light illumination is about 100 mW/cm^2. As can be seen, the current in the dark conditions increases linearly with an increase in the voltage and is symmetrical in both the forward and reverse bias directions, indicating that the contacts are ohmic. In addition, it shows a maximum current value of 0.68 μA at 10 V. However, evident negative photoconductivity has been observed for the SDB

microbelts when the light illumination is focused on the sample. At all voltage values, the current value is lower than that in the dark conditions, which is much different from the positive photoconductivity for most of the semiconductors.[49-51] The negative photoconductivity nature of the SDB microbelts make them ideal candidates for the fabrication of novel optoelectronic devices.

[Fig. 8]

Conclusions

In summary, we have successfully fabricated ultralong SDB microbelts *via* a simple self-assembly method. The length of the SDB microbelts can be readily controlled by adjusting the concentration of the initial solution as well as the aging temperature. Furthermore, the SDB microbelts show interesting optical and electrical properties, which may allow them to find potential applications in optoelectronic devices. This work provides an alternative approach to the design and fabrication of ultralong belt-like structures with rectangular cross section from small organic molecules with tunable sizes.

Acknowledgments

Financial support from Program for NSFC (51273170), International S&T Cooperation Program of Hunan Province (2013WK3036), and the Construct Program of the Key Discipline in Hunan Province is greatly acknowledged.

†Electronic supplementary information (ESI) available: Synthesis and characterization of SDB, ^{1}H NMR spectra of 4-(4,5-diphenyl-1H-imidazol-2-yl) benzyl acid (DBA) and SDB, MS spectrum of DBA, indexing results of the SDB raw powder and SDB microbelts diffraction patterns, optimized packing structure of SDB molecular dimmer and hexamer, concentration dependent UV-vis, fluorescence spectra, and fluorescence images, solid state UV-vis and fluorescence spectra. For ESI and other electronic format see DOI:

Captions

Fig. 1 (a) Photograph of SDB microbelts on glass substrate, inset showing molecular structure of SDB. (b) Photograph of the as-prepared SDB microbelts before separation. (c) Distributions of the length and width of SDB microbelts. (d, e) SEM images of SDB microbelts, inset of (e) showing the rectangular cross section. (f) Optical micrograph of a single microbelt.

Fig. 2 XRD patterns of (a) SDB raw powder and (b) SDB microbelts.

Fig. 3 FTIR spectra of (a) SDB raw powder and (b) SDB microtubes.

Fig. 4 Optical images, photographs, and distributions of the length and width of the SDB microbelts obtained under different SDB concentrations in THF, (a, b, c) 2.0 mM, (d, e, f) 3.0 mM, and (g, h, i) 4.0 mM.

Fig. 5 Optical images of the SDB microbelts obtained under different aging temperature, (a, b) 0 °C, (c) 10 °C, (d) 20 °C, (e) 30 °C, and distributions of the length of SDB microbelts, (f) 10 °C, (g) 20 °C.

Fig. 6 UV-vis absorption spectra of the SDB raw powder dispersed in water and dissolved in THF as well as the SDB microbelts dispersed in water with different lengths.

Fig. 7 Fluorescence spectra of the SDB raw powder dispersed in water and dissolved in THF as well as the SDB microbelts dispersed in water with different lengths.

Fig. 8 *I-V* measurement curves of the SDB microbelts acquired in the dark and under light illumination, inset showing the schematic diagram of a top-contacted device.

Notes and references

1 Q. Cui, Y. Zhao, J. Yao, *J. Mater. Chem.*, 2012, **22**, 4136-4140.

2 J. Oh, H. Lee, S. Mannsfeld, R. Stoltenberg, E. Jung, Y. Jin, J. Kim, J. Yoo, and Z. Bao, *PNAS.*, 2009, **14**, 6065-6070.

3 Y. Che, A. Datar, K. Balakrishnan, and L. Zang, *J. Am. Chem. Soc.*, 2007, **129**, 7234-7235.

4 Y. Zhao, H. Fu, A. Peng, Y. Ma, D. Xiao and J. Yao, *Adv. Mater.* 2008, **20**, 2859-2876.

5 X. Zhang, T. Bera, W. Liang, *J. Phys. Chem. B*, 2011, 115, 14445-14449.

6 Y. Zhao, J. Xu, A. Peng, H. Fu, Y. Ma, L. Jiang and J. Yao, *Angew. Chem. Int. Ed.*, 2008, **47**, 7301-7305.

7 A. Schwab, D. Smith, C. Rich, E. Young, W. Smith, and J. Paula. *J. Phys. Chem. B*, 2003, **107**, 11339-11345.

8 B. K. An, S. K. Kwon and S. Y. Park, *Angew. Chem. Int. Ed.*, 2007, **46**, 1978-1982.

9 A. peng, D. Xiao, Y. Ma, W. Yang, J. Yao, *Adv. Mater.*, 2005, **17**, 2070-2073.

10 K. Balakrishnan, A. S. Sayyad, G. Myhre, S. Mataka and S. Pau, *Chem. Commun.*, 2012, **48**, 11668-11670.

11 Y. Lin, Y. Qiao, X. Cheng, *J. Colloid. Interf. Sci.*, 2012, **369**, 238-244.

12 J. Li, N. Huang, D. Wang, L. Xu, Y. Huang, M. Chen, J. Tao, G. Pan, Z. Wu and L. Li, *Soft Matter*, 2013, **9**, 4642-4647.

13 J. Xu, X. Liu, J. Lv, M. Zhu, C. Huang, W. Zhou, X. Yin, H. Liu, Y. Li and J. Ye, *Langmuir*, 2008, **24**, 4231-4237.

14 M. Payne, S. Parkin, J. Anthony, C. Kuo and T. Jackson, *J. Am. Chem. Soc.*, 2005, **127**,

4986-4987.

15 Q. Niu, Y. Zhou, L. Wang, J. Peng, J. Wang, J. Pei and Y. Cao, *Adv. Mater.*, 2008, **20**, 964-969.

16 M. Law, L. Greene, J. Johnson, R. Saykally and P. Yang, *Nat. Mater.*, 2005, **4**, 455-459.

17 Z. Wang, *Adv. Mater*., 2003, **15**, 432-436.

18 Q. Tang, L. Li, Y. Song, Y. Liu, H. Li, W. Xu, W. Hu and D. Zhu, *Adv. Mater.*, 2007, **19**, 2624-2628.

19 X. Fang, S. Deng, J. Wang, X. Wang, C. Chen, Y. Li, S. Xie, R. Huang and L. Zheng, *Chem. Mater*., 2009, **21**, 5763-5771.

20 Y. Lin, Y. Qiao, X. Cheng, Y. Yan, Z. Li and J. Huang, *J. Colloid Interf. Sci.,* 2012, **369**, 238-244.

21 N. Diaz, F. X. Simon, M. Schmutz, M. Rawiso, G. Decher, J. Jestin and P. J. Mésini, *Angew. Chem. Int. Ed.*, 2005, **44**, 3260-3264.

22 L. Zhao, W. Yang, Y. Ma, J. Yao, Y. Li and H. Liu, *Chem. Commun.*, 2003, **19**, 2442-2443.

23 Y. Zhao, H. Fu, A. Peng, Y. Ma, Q. Liao, J. Yao, *Acc. Chem. Res.*, 2009, **43**, 409-418.

24 S. Yoon, I. Hwang, K. Kim and H. Choi, *Angew. Chem. Int. Ed.*, 2009, **48**, 2506-2509

25 J. Jang and J. H. Oh, *Chem. Commun.*, 2004, **7**, 882-883.

26 Y. Qiu, P. Chen and M. Liu, *J. Am. Chem. Soc.*, 2010, **132**, 9644-9652.

27 D. Lee, B. Cao, K. Jang and P. Forster, *J. Mater. Chem.*, 2010, **20**, 867-873.

28 Y. Liu, X. Zhao, B. Cai, T. Pei, Y. Tong, Q. Tang and Y. Liu, *Nanoscale*, 2014, **6**, 1323-1328.

29 L. Jiang, Y. Fu, H. Li, *J. Am. Chem. Soc.*, 2008, **130**, 3937-3941.

30 M. Huang, U. Schilde, M. Kumke, M. Antonietti and H. Cölfen, *J. Am. Chem. Soc.*, 2010, **132**, 3700-3707.

31 J. Lambrecht, T. P. Saragi, K. Onken and J. Salbeck, *ACS Appl. Mater. Inter.*, 2011, **3**, 1809-1812.

32 C. Shi, Z. Guo, Y. Yan, S. Zhu, Y. Xie, Y. S. Zhao, W. Zhu and H. Tian, *ACS Appl. Mater. Inter.*, 2013, **5**, 192-198.

33 X. Mu, W. Song, Y. Zhang, K. Ye, H. Zhang and Y. Wang, *Adv. Mater.*, 2010, **22**, 4905-4909.

34 K. Nakashima, Y. Fukuzaki, R. Nomura, R. Shimoda, Y. Nakamura, N. Kuroda, S. Akiyama and K. Irgum, *Dyes Pigments.*, 1998, **38**, 127-136.

35 N. Fridman, M. Kaftory, Y. Eichen and S. Speiser, *J. Photochem. Photobio. A: Chem.*, 2007, **188**, 25-33.

36 K. Feng, F. Hsu, D. Van Der Veer, K. Bota and X. Bu, *J. Photochem. Photobio. A: Chem.*, 2004, **165**, 223-228.

37 K. Nakashima, *Biomed. Chromatogr.*, 2003, **17**, 83-95.

38 O. Al-Dirbashi, J. Qvarnstrom, K. Irgum and K. Nakashima, *J. Chromatogr. B: Biomed. Sci. Appl.*, 1998, **712**, 105-112

39 Y. Zhao, D. Xiao, W. Yang, A. Peng and J. Yao, *Chem. Mater.*, 2006, **18**, 2302-2306.

40 Y. Zhao, W. Yang and J. Yao, *Phys. Chem. Chem. Phys.*, 2006, **8**, 3300-3303.

41 Y. Zhao, W. Yang, D. Xiao, X. Sheng, X. Yang, Z. Shuai, Y. Luo and J. Yao, *Chem. Mater.*, 2005, **17**, 6430-6435.

42 B. Delley, *J. Chem. Phys.*, 1990, **92**, 508-517;

43 B. Delley, *J. Chem. Phys.*, 2000, **113**, 7756-7764.

44 Q. Liao, Z. Nie, H. Chen, X. Luo, Y. Gao and H. Li, *J. Appl. Polym. Sci.*, 2012, **126**, 1146-1151.

45 Z. Chen, U. Baumeister, C. Tschierske and F. Würthner, *Chem. Eur. J.*, 2007, **13**, 450-465.

46 H. Fu, J. Yao, *J. Am. Chem. Soc.*, 2001, **123**, 1434-1439.

47 M. Ornatska, S. Peleshanko, B. Rybak, J. Holzmueller and V. V. Tsukruk, *Adv. Mater.*, 2004, **16**, 2206-2212.

48 M. Huang, U. Schilde, M. Kumke, M. Antonietti and H. Cölfen, *J. Am. Chem. Soc.*, 2010, **132**, 3700-3707.

49 X. Zhang, J. Jie, W. Zhang, *Adv. Mater*., 2008, **20**, 2427-2432.

50 P. Liu, Y. Ma, W. Cai, *Nanotechnology*., 2007, **18**, 205704.

51 N. Ai, Y. Zhou, Y. Zheng, *Org. Electron.*, 2013, **14**, 1103-1108.

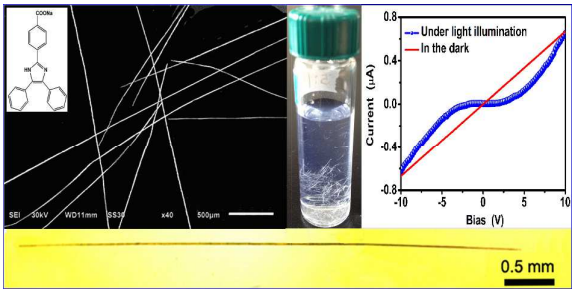

Enty.

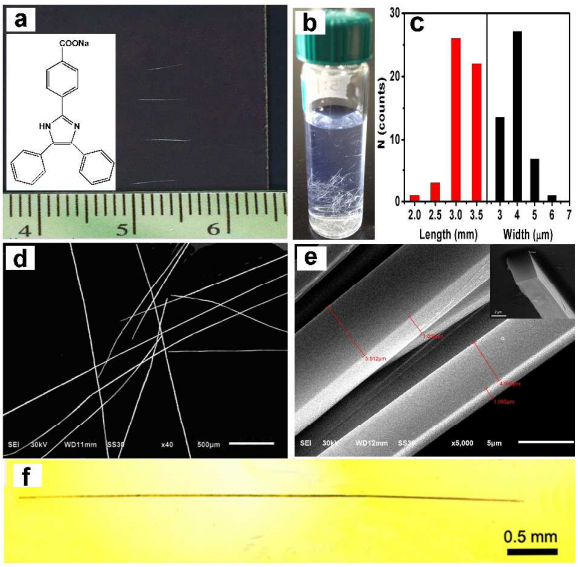

Fig.1

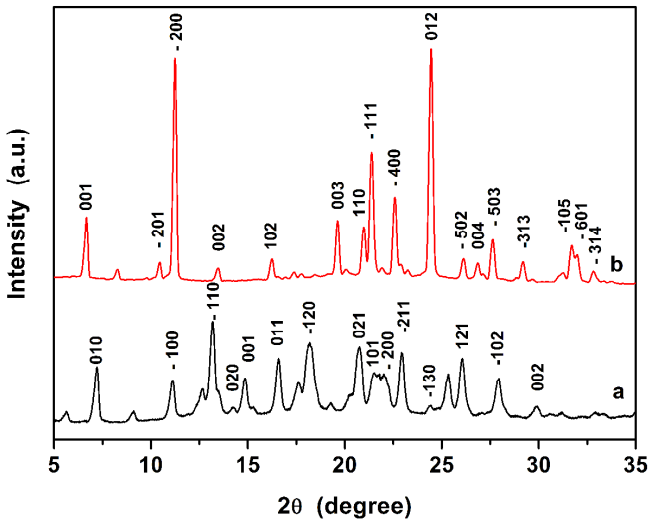

Fig.2.

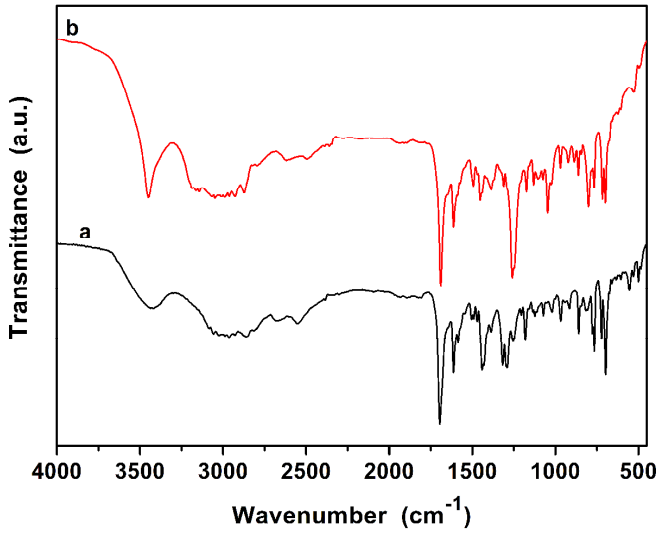
b
a
Transmittance (a.u.)
4000 3500 3000 2500 2000 1500 1000 500
Wavenumber (cm-1)

Fig.3

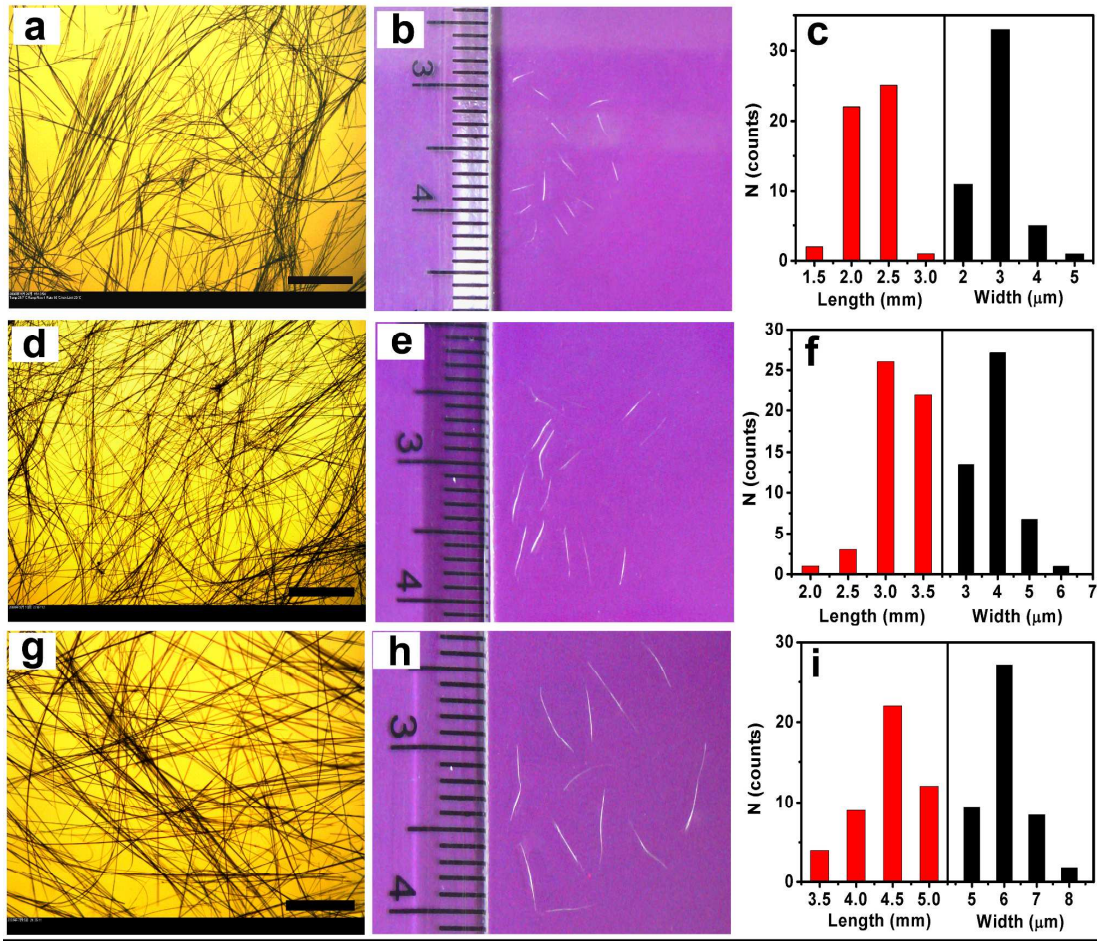
a
b
c
d
e
f
g
h
i
N (counts)
Length (mm)
Width (μm)

Fig.4.

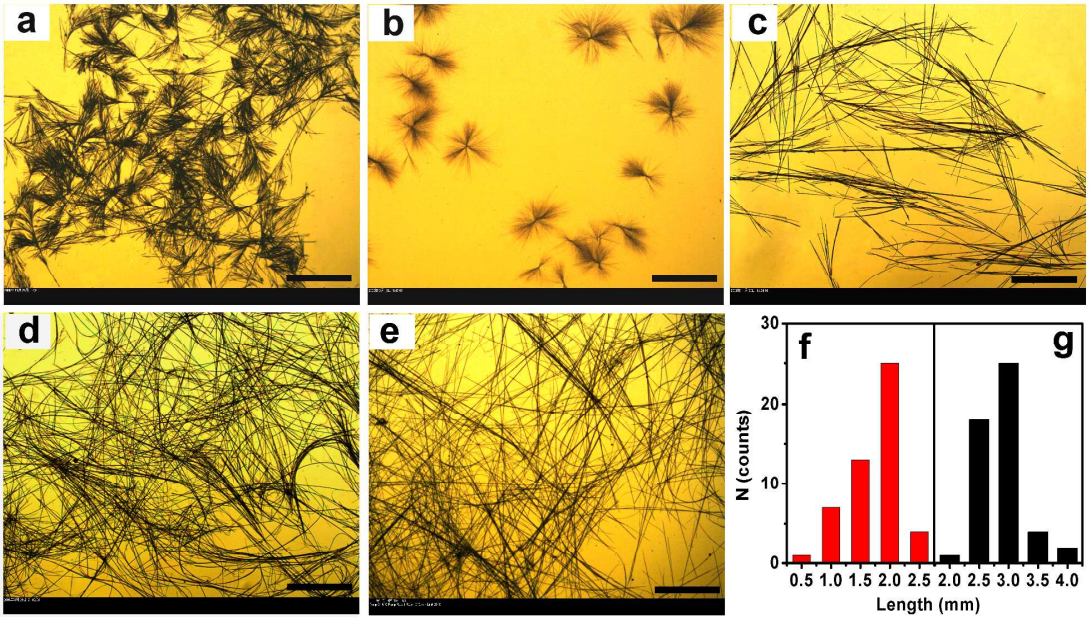
a
b
c
d
e
f
g
N (counts)
Length (mm)
0
10
20
30
0.5 1.0 1.5 2.0 2.5 2.0 2.5 3.0 3.5 4.0

Fig.5.

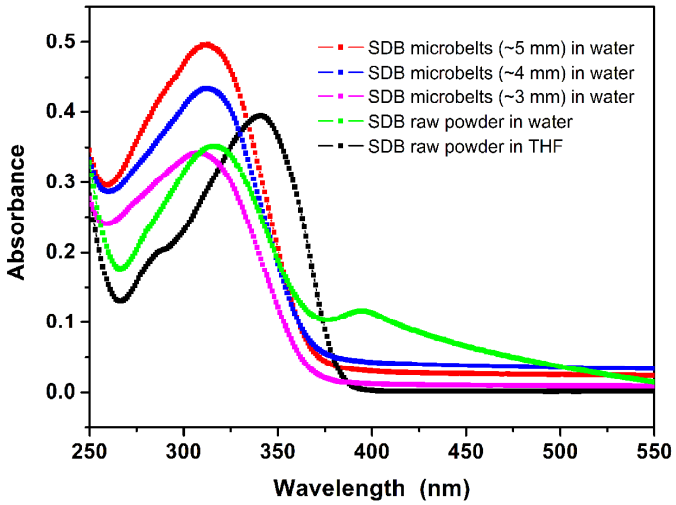
SDB microbelts (~5 mm) in water
SDB microbelts (~4 mm) in water
SDB microbelts (~3 mm) in water
SDB raw powder in water
SDB raw powder in THF
Absorbance
Wavelength (nm)
0.0
0.1
0.2
0.3
0.4
0.5
250
300
350
400
450
500
550

Fig.6.

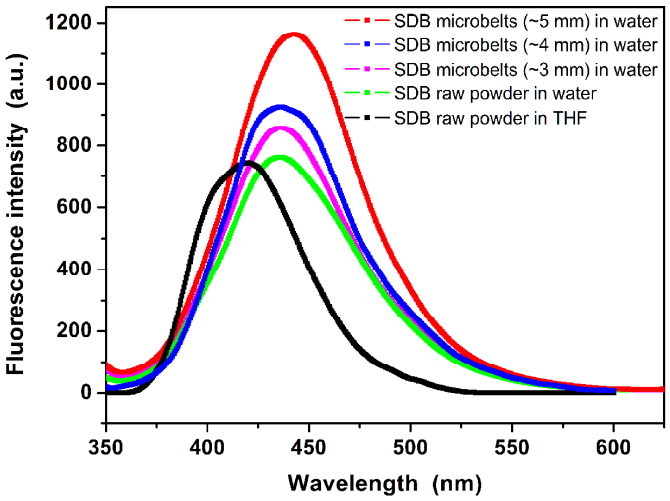
SDB microbelts (~5 mm) in water
SDB microbelts (~4 mm) in water
SDB microbelts (~3 mm) in water
SDB raw powder in water
SDB raw powder in THF
Fluorescence intensity (a.u.)
Wavelength (nm)
0
200
400
600
800
1000
1200
350
400
450
500
550
600

Fig.7

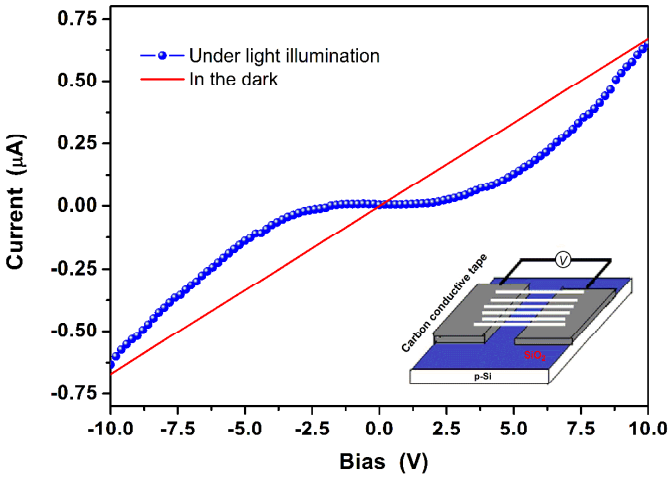
Under light illumination
In the dark
Current (μA)
Bias (V)
0.75
0.50
0.25
0.00
-0.25
-0.50
-0.75
-10.0
-7.5
-5.0
-2.5
0.0
2.5
5.0
7.5
10.0
Carbon conductive tape
V
SiO2
p-Si

Fig.8

Table of contents entry

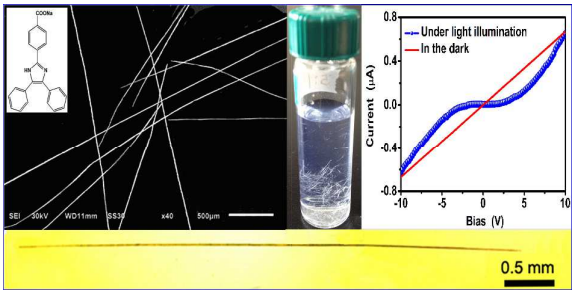

Ultralong SDB microbelts with interesting optical and electrical properties were successfully fabricated by the poor solvent mediated self-assembly method.